Monte Carlo Dynamic Analysis for Lunar Module Landing Loads

D. H. MERCHANT* AND D. T. SAWDY†
The Boeing Company, Houston, Texas

A comprehensive Monte Carlo dynamic analysis was performed to verify the structural integrity of the Apollo Lunar Module for lunar landing. A fundamental consideration of this Monte Carlo analysis was to synthesize a mathematical model by combining fixed data quantities with random variables. The mathematical model was used to obtain numerous simulations of the landing maneuver and to compute the resulting external and internal structural loads. These analytical loads were then treated statistically, by means of two separate confidence limit calculations, to determine exceedance probabilities associated with the loads. A general discussion of the methodology used for the analysis is presented in this paper, along with a summary of the mathematical idealization and some typical internal loads with their corresponding exceedance probabilities.

Nomenclature

Statistical techniques

F = randomly varying load quantity
F_α = unknown $\alpha \times 100$ percentile value of load quantity
$\hat{F}_\alpha$ = point estimate of F_α
K = normal variate corresponding to arbitrary probability
K_α = tabulated normal variate corresponding to probability level α
K_γ = tabulated normal variate corresponding to confidence level γ
N = number of cases in sample
S = unbiased sample estimate of standard deviation
$\bar{X}$ = unbiased sample estimate of mean
X_α = confidence limit related to F_α and determined from finite sample
α = load level probability
γ = confidence level probability
μ = mean of normally distributed load quantity
σ = standard deviation of normally distributed load quantity

Landing dynamics

$\mathbf{A}_{Ri}$ = rotational inertial acceleration of ith mass point
$\mathbf{A}_{Ti}$ = translational inertial acceleration of ith mass point
$\{DL\}$ = matrix of external dynamic forces and moments
$\mathbf{DL}_i$ = external dynamic force on ith mass point
$\mathbf{DM}_i$ = external dynamic moment on ith mass point
$\mathbf{F}_{Ai}$ = external force applied directly to ith mass point
$\mathbf{F}$ = total force applied to LM centroid
GF_j = generalized force for jth elastic vibrational mode
$\mathbf{g}_L$ = acceleration of lunar gravity
$\tilde{I}$ = total LM inertia tensor
$\{IL\}$ = matrix of internal structural loads
$\tilde{J}_i$ = rotational mass inertia tensor of ith mass point
$\mathbf{L}_i$ = constant position vector from LM centroid to ith mass point
$\mathbf{M}$ = total moment applied to LM centroid
$\mathbf{M}_{Ai}$ = external moment applied directly to ith mass point
m_i = mass of ith mass point
M_j = generalized mass of jth elastic vibrational mode
M_T = total LM mass
$\ddot{q}_j, \dot{q}_j, q_j$ = generalized modal acceleration, velocity, and displacement for jth mode
$\ddot{\mathbf{R}}$ = translational inertial acceleration of LM centroid
$[SM]$ = stress matrix relating internal loads to external loads
$\{\ddot{X}_e\}$ = matrix of relative elastic translational and rotational accelerations
$\ddot{\mathbf{X}}_{ei}$ = relative elastic translational acceleration of ith mass point
ζ_j = viscous damping ratio for jth mode
$\ddot{\boldsymbol{\theta}}_{ei}$ = relative elastic rotational acceleration of ith mass point
$[\phi]$ = matrix of natural mode shapes by column
$\boldsymbol{\omega}$ = rotational inertial velocity of LM centroid
$\dot{\boldsymbol{\omega}}$ = rotational inertial acceleration of LM centroid
ω_j = frequency (rad/sec) of jth mode

Introduction

THE dynamic loads analysis described herein was used to verify the structural adequacy of the Lunar Module (LM) to withstand the loading environment for the first Apollo lunar landing.[1,2] This analysis was performed at the request of the Structures and Mechanics Division of the NASA Manned Spacecraft Center (NASA-MSC) and with the cooperation of the Grumman Aerospace Corporation (GAC). Since this design verification analysis was begun less than one year prior to the Apollo 11 mission, a detailed three-dimensional structural model of the LM, prepared by GAC, was available. In addition, results of full-scale LM dynamic test programs, of Descent Propulsion System (DPS) engine test firings, of landing-gear component tests, and of a series of simulated flights to touchdown were available for incorporation into the mathematical model. Finally, NASA-MSC had developed accurate descriptions of the lunar surface features of the candidate landing sites. Thus sufficient descriptive data were available to justify a comprehensive dynamic loads analysis.

There are at least two basic methods for calculating dynamic loads to verify a structural design. One method is to calculate loads based on discrete values selected by judgment from the entire range of possible input data parameters. The maximum load from this parameter-variation study is then assumed to be the design limit load. One difficulty with this method is that the resulting maximum load may be unduly conservative. A more serious difficulty in applying this method to a complex dynamics problem is that, if experience and judgment are insufficient to identify the combination of parameters yielding maximum loads, the number of cases required to investigate the various possible

Presented at the AIAA/ASME 11th Structures, Structural Dynamics, and Materials Conference, Denver, Colo., April, 1970; submitted May 27, 1970; revision received September 28, 1970. This work was supported by NASA under Contract NASw-9-1650. The computer programs developed for and used in this analysis were written by D. L. Graves and J. F. Murray of The Boeing Company.

* Specialist Engineer, Structures & Dynamics, Aerospace Group. Member AIAA.
† Specialist Engineer, Structures & Dynamics, Aerospace Group.

input combinations may well be prohibitive. For example, if eight input parameters have only three discrete values each, the number of cases required to investigate each possible combination is $(3)^8$, or more than 6000 cases.

A second method is to calculate loads based on values selected at random from the probability distributions of the input data parameters. The calculated internal loads are then analyzed statistically to yield a probability of occurrence corresponding to each load. By this method, the number of cases required to determine design verification loads may be as few as 100 cases. This analysis procedure is generally known as the Monte Carlo method.[3,4] The purpose of this paper is to present the technical methodology involved in the application of the Monte Carlo method to the LM lunar landing dynamic loads analysis.

Monte Carlo Method

The Monte Carlo method as applied to the present dynamics problem was a simulation of the loading conditions actually encountered, in a large number of landings on a surface having specified properties, by a vehicle having specified characteristics. The analysis had four general aspects: 1) formulating the mathematical idealization of the random phenomenon, 2) generating the sample values of the random variables, 3) calculating observed values of the random phenomenon, and 4) statistically analyzing the observed values.

A fundamental consideration of this lunar landing analysis was to synthesize a mathematical model by combining deterministic and probabilistic variables. Typical examples of deterministic variables were vehicle mass and geometry data, load-stroke properties of landing-gear struts, DPS thrust-decay characteristics, and lunar soil properties. The randomness of the landing maneuver was represented by the following probabilistic variables: initial vehicle translational and rotational velocities, initial angular orientations, initial position of the LM centroid relative to the idealized lunar surface. The mathematical model was developed by assigning values to the deterministic variables and probability distributions to the random variables. Specific sets of initial conditions were then computed by means of a random number generator. From these initial conditions, the dynamic responses and corresponding structural loads were calculated for the idealized vehicle.

A major consideration in the general application of the Monte Carlo analysis is to develop and apply techniques for reducing the variance of the observed values and for determining the statistical errors. The purpose of the several variance-reducing techniques discussed by Kahn[4] is to reduce the statistical error without increasing the number of simulations required. For the present Monte Carlo lunar landing analysis, none of these techniques was found to be advantageous. However, statistical techniques involving parametric confidence limits were effectively used. By means of parametric extrapolation of the calculated loads, probability statements were made for loads with relatively small probabilities of exceedance.

Statistical Techniques

The Monte Carlo analysis yields results equivalent to the landing of an idealized vehicle on an idealized lunar surface; these results may be treated statistically as measured data. The fundamental statistical quantities of interest are the point estimates and confidence interval estimates for each internal dynamic load quantity. These statistical computations in effect relate the calculated dynamic loads of the finite sample with the unknown loads of the infinite population of the mathematical model. It should be emphasized that such probability statements strictly concern only the loads of the idealized model, and that the application of these statements to the actual physical system requires engineering judgment.

The basic statistical output from a Monte Carlo analysis for dynamic loads is the probability that a given load will not be exceeded. For example, the design load in a certain member may be that load which will be exceeded, on the average, only one time in 100 landings. That is, by definition,

$$Pr\cdot[F < F_{0.99}] = 0.99 \tag{1}$$

With a finite sample size, the exact determination of the true $\alpha \times 100\%$ load is not possible. However, it is possible to obtain point estimates of this load quantity. For an infinitely large sample, the point estimates $(\hat{F}_\alpha)$ coincide with the true $\alpha \times 100\%$ load (F_α). For a finite sample, the point estimates exhibit statistical variability. Since this variability is well defined probabilistically, confidence limits may be calculated to provide conservative estimates of the true load.

The one-sided confidence limit for the $\alpha \times 100\%$ load is represented by the following probability statement for confidence level (γ):

$$Pr\cdot[F_\alpha < X_\alpha] = \gamma \tag{2}$$

Here X_α is a value, determined from the finite sample, which may be expected to exceed the true $\alpha \times 100\%$ load, on the average, $\gamma \times 100\%$ of the time. The confidence limit (X_α) and the point estimate $(\hat{F}_\alpha)$ may be calculated either from no assumed knowledge concerning the underlying probability distribution of the load quantity or from assumed complete knowledge of the underlying probability distribution. These two calculations are denoted, respectively, as nonparametric and parametric estimation methods.

The nonparametric point estimate of the $\alpha \times 100\%$ load is obtained from the sample of N loads, ordered according to magnitude, as the load which is not exceeded $\alpha\cdot N$ times. For example, the estimate of the 95% load in a sample of 100 cases is that load which is exceeded by only five other loads.

The nonparametric confidence limit is obtained from the binomial sampling theory for quantiles. The only required assumption is that a true probability distribution for the loads exists. By definition, the probability is α that any load in a random sample does not exceed the true $\alpha \times 100\%$ load. In a sample of N independent trials, let i represent the number of loads less than or equal to the true $\alpha \times 100\%$ load. Then, the probability that i equals n is defined by the binomial probability law:

$$Pr\cdot[i = n] = [N!/n!(N - n)!]\alpha^n\cdot(1 - \alpha)^{N-n} \tag{3}$$

The confidence limit is then obtained from the following probability statement:

$$Pr\cdot[i < n] = \gamma \tag{4}$$

where n is the number of load cases in the sample which do not exceed X_α in Eq. (2). From Eqs. (3) and (4), the required relation between the calculated probability level (α_c) and the confidence level (γ) is given by

$$\gamma = \sum_{i=0}^{n-1} [N!/i!(N - i)!]\alpha_c^i\cdot(1 - \alpha_c)^{N-i} \tag{5}$$

This relation is valid throughout the entire range of the variables.

The parametric confidence interval used in the present analysis is based on the assumption that the underlying probability distribution of the load quantity is either normal or transformed normal. A particularly useful transformation for loads data is logarithmic. Loads which follow the normal probability law after the logarithmic transformation are said to be log-normally distributed.

If a load quantity can be assumed normally distributed with mean equal to μ and standard deviation equal to σ, then

the true $\alpha \times 100\%$ load can be expressed as

$$F_\alpha = \mu + K_\alpha \cdot \sigma \tag{6}$$

where

$$\alpha = [1/(2\pi)^{1/2}] \int_{-\infty}^{K\alpha} e^{-t^2/2} dt$$

The corresponding point estimate of this load is given by

$$\hat{F}_\alpha = \bar{X} + K_\alpha \cdot S \tag{7}$$

These sample estimates of the mean and standard deviation are unbiased; i.e., the mean values of these estimators equal the true population mean and standard deviation. Notice that F_α is not estimated by the $\alpha \times 100\%$ order statistic as is done for the nonparametric method. Any load in the infinite population may be estimated from a finite sample by

$$\hat{F} = \bar{X} + K \cdot S \tag{8}$$

The distribution of $\hat{F}$ is derived as follows for a normally distributed load quantity with mean equal to μ and standard deviation equal to σ.[5] The sample mean and the sample standard deviation are independent random variables. The sample mean is distributed as follows:

$$\bar{X} \sim \text{Normal [mean} = \mu, \text{ std. dev.} = \sigma/(N)^{1/2}]$$

The sample standard deviation is approximately distributed as follows for N greater than 50:

$$S \sim \text{Normal } \{\text{mean} = \sigma, \text{ std. dev.} = \sigma/[2(N-1)]^{1/2}\}$$

Combining the two independent normally distributed random variables yields

$$\hat{F} \sim \text{Normal } \{\text{mean} = \mu + K \cdot \sigma, \text{ std. dev.} = \sigma[(K^2 + 2)/2(N-1)]^{1/2}\}$$

The general confidence statement of Eq. (2) may be expressed as follows:

$$Pr \cdot [F_\alpha < \hat{F}] = \gamma \tag{9}$$

Equation (9) implies that

$$-K_\gamma = [F_\alpha - (\mu + K \cdot \sigma)]/\sigma[(K^2 + 2)/2(N-1)]^{1/2} \tag{10}$$

where

$$\gamma = [1/(2\pi)^{1/2}] \int_{-K\gamma}^{\infty} e^{-t^2/2} dt$$

Substituting Eq. (6) into Eq. (10) and solving for the appropriate root of K yields

$$K_c = [K_\alpha + (K_\alpha^2 - a \cdot b)^{1/2}]/a \tag{11}$$

where

$$a = 1 - K_\gamma^2/2(N-1), \; b = K_\alpha^2 - K_\gamma^2/(N-1)$$

From Eqs. (8), (9), and (11), the probability statement for the parametric confidence limit may be given by

$$Pr \cdot [F_\alpha < \bar{X} + K_c \cdot S] = \gamma \tag{12}$$

The parametric statistical estimates are based on the assumption that the underlying probability distributions of the load quantities are either normal or transformed normal. This assumption can be investigated by means of statistical goodness-of-fit tests such as the chi-square test[6] and the Kolmogorov-Smirnov test.[7]

The nonparametric confidence limit permits probability statements to be made for each calculated load in the sample. These statements are valid regardless of either the underlying probability distribution of the loads or the sample size. However, if the underlying loads distribution can be assumed with reasonable certainty to be either normal or transformed normal, then the parametric confidence limit may be used to obtain loads somewhat larger than those calculated in the sample. For example, for a sample of 100 cases, the 97% load is the largest load that can be estimated with a 95% nonparametric confidence. However, the 99.5% load could be reasonably estimated with the same confidence from the same sample, if the parametric confidence limit could be applied.

Landing Dynamics

The three-dimensional dynamic response of the LM to the landing maneuver was calculated by means of a comprehensive digital computer program. The basic rigid-body response portion of this program, developed by the Structures and Mechanics Division of NASA-MSC,[8] integrates the rigid-body equations of motion forced by the stroking of the landing-gear struts. The strut stroking is obtained through motion of the strut attachment points relative to the footpads which are constrained by the rigid lunar surface. In the elastic response portion of the program, the flexibility of the LM structure is represented by free-free elastic vibrational modes. This separation of the rigid-body and elastic responses is acceptable because the Coriolis acceleration terms are negligible for the range of LM rotational velocities encountered. Coupling between the rigid-body and modal equations is effected only through forces resulting from elastic displacements and velocities of the strut attachment points.

The digital program accepts as input the initial velocities and orientations selected by the random number generator, in addition to the randomly selected initial position over the idealized lunar surface. Other input data describing the physical characteristics of the LM include the following: vehicle geometry, mass and inertia data, load-stroke properties of landing gear and crushable DPS nozzle, and DPS thrust-decay characteristics.

Integration of the equations of motion begins with the randomly generated initial position, orientation, and velocity; the initial position of the LM centroid has the footpad nearest the surface located approximately 5 ft above the surface. The LM motion is then calculated under the influence of lunar gravity and DPS thrust until impact occurs. After impact, additional forces are transmitted through the landing gear and the DPS nozzle from the lunar surface, which is assumed infinitely resistant to penetration and sliding. The crushable honeycomb cartridges in the landing gear struts, idealized as weightless nonlinear springs, are the primary mechanisms for dissipating the initial energy. The bouncing motions of the LM are then calculated until the achievement of a specified minimum energy level automatically terminates the program.

Two orthogonal coordinate systems were used to describe the LM motions during the landing maneuver: the gravity-surface inertial coordinate system and the LM body-fixed centroidal coordinate system. By means of Euler angles, the LM body-fixed coordinate system was oriented with respect to the inertial coordinate system. For convenience, the basic LM rigid-body equations of motion and the dynamic loads equations are shown here in vector notation. All vector quantities are resolved into the body-fixed coordinate system, except those whose symbols are followed by (I).

The translational inertial accelerations of the LM centroid are given in the inertial coordinate system by

$$\ddot{\mathbf{R}}(I) = (1/M_T)\mathbf{F}(I) \tag{13}$$

The rotational inertial accelerations of the LM centroid are given in the body-fixed coordinate system by Euler's equations of motion:

$$\dot{\boldsymbol{\omega}} = \tilde{I}^{-1}\mathbf{M} - \tilde{I}^{-1}[\boldsymbol{\omega} \mathrm{X} \tilde{I}\boldsymbol{\omega}] \tag{14}$$

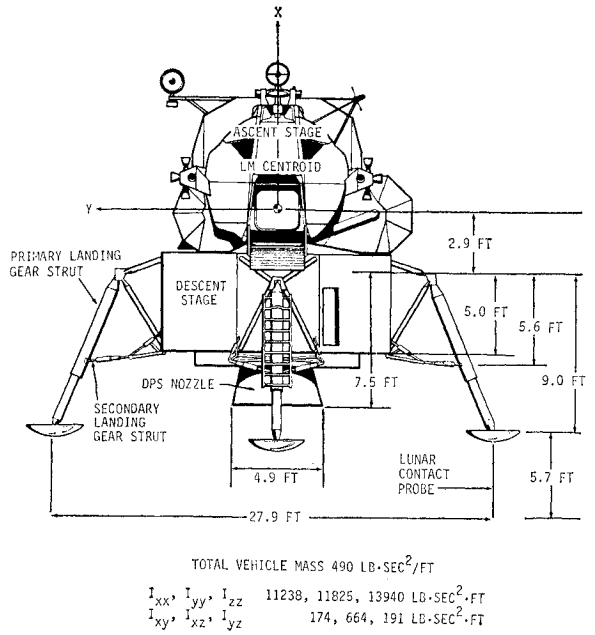

Fig. 1 Typical LM geometry and nominal mass properties.

The elastic response equations are the standard modal equations with viscous damping. These linear equations utilize the orthogonality properties of the undamped normal modes to transform from physical coordinates into generalized modal coordinates. The resulting uncoupled elastic response equations, with viscous modal damping superimposed, are of the form

$$M_i\ddot{q}_i + 2\zeta_i\omega_i M_i\dot{q}_i + \omega_i^2 M_i q_i = GF_i \qquad (15)$$

The generalized forces consist of the contributions to each mode of the forces applied to the structure by the landing gear stroking, the DPS nozzle crushing, and the DPS thrust. The total elastic translational and rotational accelerations of the primary masses in body-fixed coordinates are defined as the linear combinations of the contributions of the individual undamped normal mode shapes:

$$\{\ddot{X}_e\} = [\phi]\{\ddot{q}\} \qquad (16)$$

The use of free-free modes in the elastic response calculations is mathematically rigorous despite the fact that the attachment points of the landing-gear struts are partially constrained while the footpads are in contact with the lunar surface. This is due to the exact equivalence between kinematic constraints and force constraints. In the landing dynamics program, the kinematic constraints at the footpads are converted to equivalent externally applied forces at the landing-gear attachment points, without changing the mechanical impedance of the attachment points.

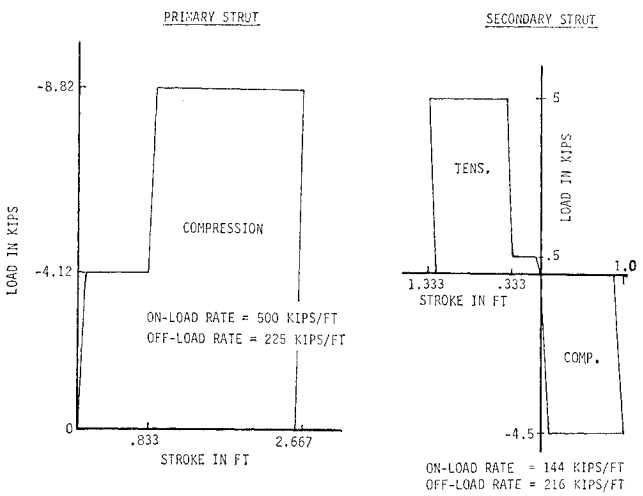

Fig. 2 Force-stroke characteristics for LM landing gear struts.

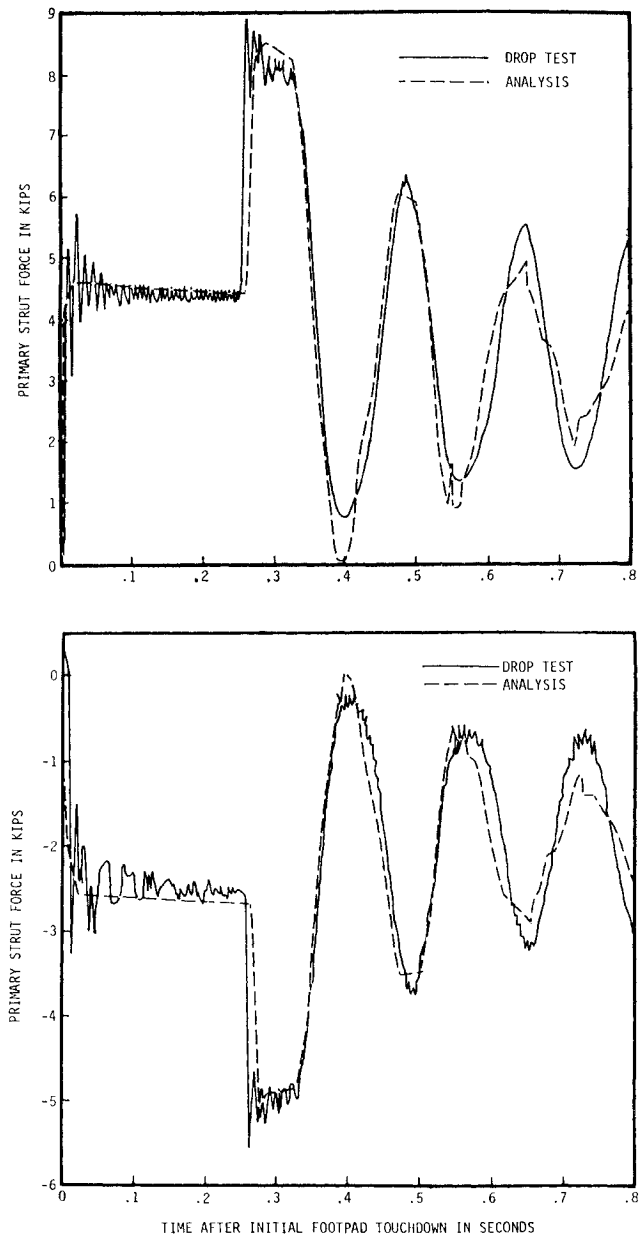

Fig. 3 Force in right (+Y) primary strut.

The primary desired output of a dynamic loads analysis is the internal load in each critical structural member. When these internal loads may be expressed mathematically as functions of the external dynamic loads, the desired output may be achieved. External loads are the total dynamic forces and moments acting on the individual structural mass points. External dynamic forces on the ith mass point are given by

$$\mathbf{DL}_i = \mathbf{F}_{A_i} - m_i\mathbf{A}_{T_i} \qquad (17)$$

The translational inertial acceleration of the ith structural mass point (including the effect of gravity) is

$$\mathbf{A}_{T_i} = \ddot{\mathbf{R}} + \mathbf{g}_L + \dot{\omega}\mathbf{XL}_i + \omega\mathbf{X}\omega\mathbf{XL}_i + \ddot{\mathbf{X}}_{e_i} \qquad (18)$$

External dynamic moments acting on each individual mass point having rotational degrees of freedom are

$$\mathbf{DM}_i = \mathbf{M}_{A_i} - \tilde{J}_i \mathbf{A}_{R_i} \tag{19}$$

The rotational inertial acceleration of the ith mass point is

$$\mathbf{A}_{R_i} = \dot{\boldsymbol{\omega}} + \ddot{\boldsymbol{\theta}}_{e_i} \tag{20}$$

The desired internal loads in critical structural members are then related to the external dynamic forces and moments by a stress matrix as follows:

$$\{IL\} = [SM]\{DL\} \tag{21}$$

Mathematical Model

A schematic view showing the general configuration of the LM and indicating some geometrical relationships is presented in Fig. 1. The total LM mass properties for the estimated nominal landing weight, excluding the weight of the landing gear, are also listed in Fig. 1. The LM structural characteristics were represented by free-free elastic vibrational modes computed from a 280 degree-of-freedom GAC stiffness matrix. Since the local resonances of the LM major mass items were below 30 cps, the use of the 50 modes having frequencies below 55 cps was considered sufficient to yield accurate structural dynamic responses.

The honeycomb crushing forces of the landing gear honeycomb cartridges consist of both a static force component, which is dependent on stroking displacement, and a dynamic force component, which is dependent on stroking velocity. The static crush levels, presented in Fig. 2, were determined by GAC from honeycomb cartridge component crushing tests performed in a vacuum. The dynamic force components and the on-load and off-load spring rates were determined by comparison of analytical forces with forces obtained experimentally from a full-scale LM drop test.[9] This drop was a symmetric, vertical drop with all footpads impacting simultaneously (at 4.6 fps) and prevented from sliding on the rigid surface. Time-history plots for the most significant forces, the longitudinal and radial components of the primary strut forces, are shown in Fig. 3 for a typical landing gear. The agreement between test and analysis is seen to be excellent.

The LM free-fall motion immediately preceding footpad touchdown is modified by the decaying DPS thrust. The thrust decay characteristics of the DPS engine were measured during engine shutdown tests performed at the White Sands Test Facility. The curve of the -3σ thrust-decay transient was described mathematically as a piecewise continuous function with parameters determined from a least-squares curve fit.

The lunar surface elevation data were generated and provided by the NASA-MSC Mapping Sciences Laboratory. Elevation tables and corresponding LM tilt angle distributions, for each of the five candidate sites for the first Apollo lunar landing mission, were determined from a photometric technique applied to monoscopic Lunar Orbiter photographs. This technique determines slope at a point from a photometric analysis involving the relative brightness of solar light rays reflected by the lunar surface. Elevations are obtained by integrating the calculated slopes along radial lines through the zero phase point, which is the location of the camera shadow on the lunar surface. Elevation tables are determined independently for the smallest unit of the candidate site, which is approximately 680 ft^2.

An elevation table, determined by the MSC photometric technique for a typical unit, was selected as the mathematical

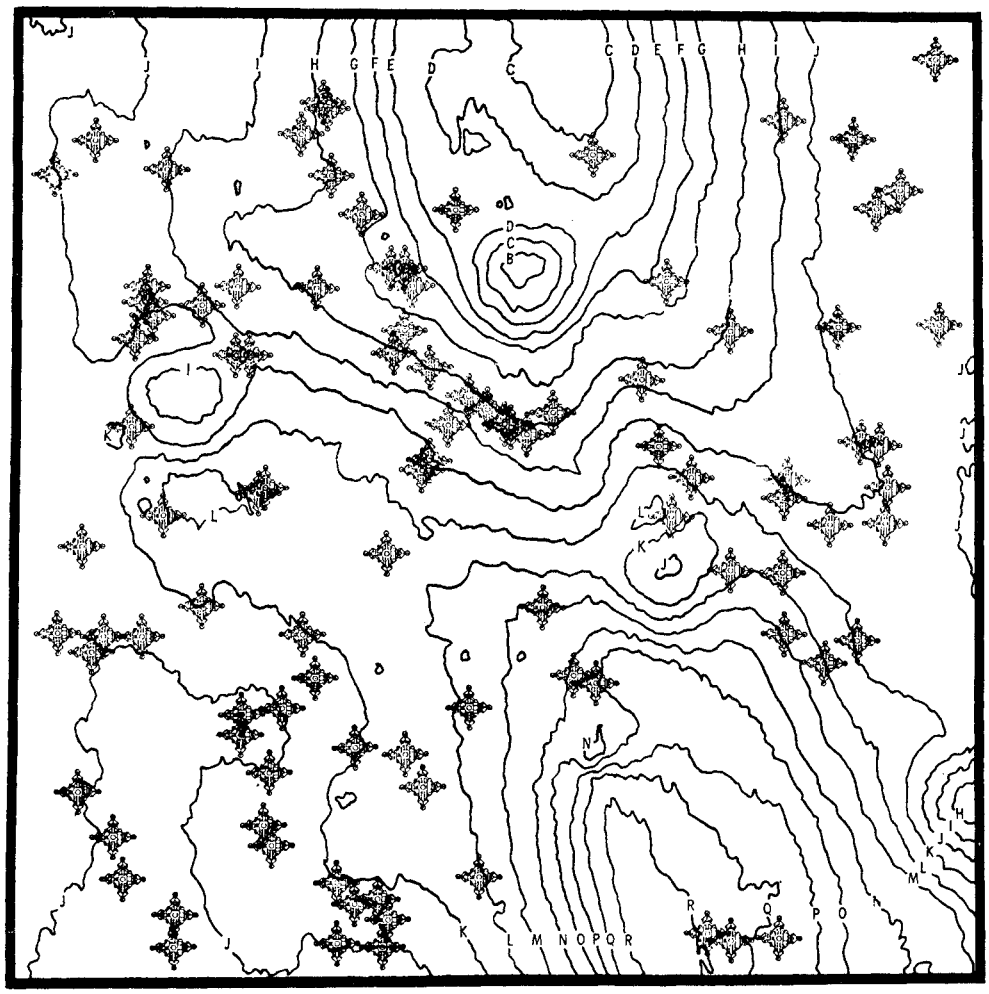

Fig. 4 Elevation contour map for idealized lunar surface.

Table 1 Initial conditions at probe contact (rate-of-descent mode)

Variable	Units	Distribution
Vertical velocity ($\dot{X}$)	fps	$N(\mu = -3.67, \sigma = 0.75)$
Lateral velocity ($\dot{Y}$)	fps	$N(\mu = 0.05, \sigma = 0.84)$
Forward velocity ($\dot{Z}$)	fps	$N(\mu = 0.22, \sigma = 0.86)$
Body yaw rate (ω_x)	deg/sec	$N(\mu = 0.02, \sigma = 0.06)$
Body pitch rate (ω_y)	deg/sec	$N(\mu = 0.21, \sigma = 0.92)$
Body roll rate (ω_z)	deg/sec	$N(\mu = -0.04, \sigma = 0.62)$
Euler pitch angle (θ_y)	deg	$N(\mu = 0.25, \sigma = 1.55)$
Euler roll angle (θ_z)	deg	$N(\mu = 0.04, \sigma = 1.60)$

idealization of the lunar surface. Figure 4 shows the individual landing positions for the Monte Carlo loads analysis plotted on an MSC contour map of the selected 680-ft² unit (MSC site 3, unit 123-534-6). The contour interval is approximately four ft, and the LM symbols are plotted to scale. As shown on the contour map, no landings were permitted in the areas where the slopes exceed 12°, which was the minimum value of the stability envelope. By this means, the judgment of the LM pilots in selecting the touchdown location was included in the mathematical idealization.

The gross elevation table of the selected unit consists of elevations of points spaced at constant intervals of about 2 ft across the surface. For efficiency in the landing dynamics computer program, the gross elevation table was divided into 100 local elevation tables centered around the randomly generated centroidal landing coordinates. The point elevations from the local tables were converted into a continuous surface by fitting a hyperbolic paraboloid through the elevations of the four grid points adjacent to each footpad. Primarily because of inadequate data regarding lunar soil properties, the lunar surface was conservatively assumed infinitely resistant to both penetration and sliding.

Random Selection of Initial Conditions

The landing phase of the lunar mission begins at an altitude of approximately 500 ft above the lunar surface. At this point, the crew makes the final assessment of the predetermined landing site and selects one of three basic landing modes: automatic, rate-of-descent, or manual. For the semiautomatic rate-of-descent mode, the pilot commands the vertical velocity in increments of 1 fps and supplies manual inputs for horizontal velocity and angular orientation. In the absence of manual control inputs, the commanded velocities and orientations are automatically maintained. When one of the three lunar-contact probes touches the lunar surface, two lunar-contact lights on the control panel illuminate; then either crew member manually shuts off the DPS engine. Although the final choice of landing procedure for any given mission is left to the crew, the rate-of-descent mode with manual engine shutdown is considered nominal.

The random state vector at probe contact was described by probability distributions for the individual components of translational and rotational velocity and angular orientation. The basic data for the statistical descriptions were provided by a GAC lunar landing simulation study.[10] The simulated landings were conducted by astronauts and test pilots in a simulated LM crew station. The values of the state vector displayed on the control panel during the simulated landings were computed continuously from the manual inputs supplied by the pilot. In addition, an external visual display of a lunar surface model simulated the pilot's view from the LM window during landing.

The required velocity components and Euler angles at probe contact were generated by GAC for 48 simulated landings by each of four pilots. A statistical analysis conducted by GAC determined that the individual components were all mutually independent and normally distributed. For the nominal rate-of-descent simulation, the means and standard deviations of all variables for the individual pilots were combined to yield the composite parameter values listed in Table 1. The pilot reaction time, defined as the time between probe-contact light illumination and the depressing of the engine-off button, is a critical factor in determining footpad impact velocity as shown in Fig. 5. Therefore, a minimum pilot reaction time was conservatively assumed with small variation about a mean of 0.2 sec.

A digital computer program was used to select the sets of initial conditions for the Monte Carlo analysis.[11] This program calculates a sequence of numbers which, for the purposes of the Monte Carlo analysis, accurately simulates a sequence of random variates having a normal or uniform distribution. The program was verified by investigating the generated random numbers with statistical hypothesis tests. The distributions of individual sequences were tested by means of the standard chi-square hypothesis test. A modified chi-square test for serial correlation was used to verify that a given number in the sequence is unrelated to any other number in the sequence. These first level chi-square tests for numerous sequences were complemented by second-level Kolmogorov-Smirnov tests of the chi-square probabilities. These hypothesis tests indicated that calculated sequences of pseudo-random numbers exhibit the statistical properties required for the Monte Carlo analysis.

Results

The detailed dynamic responses of the LM mathematical model were determined for each of the 100 lunar landing cases by the landing dynamics computer program. All of the simulated landings were assured to be stable by the selection of landing sites with slopes within the 12° stability envelope. General landing indicators, such as maximum stroke of each primary landing gear strut and LM vertical velocity at footpad impact, were monitored to characterize each simulated landing. The upper crush levels of the primary struts were attained 186 times out of 400 possible footpad strokes. Nearly half of the vertical impact velocities occurred between 7.0 and 7.3 fps; this uniformity of the impact velocity is illustrated in Fig. 5 for the assumed minimum pilot reaction time of approximately 0.2 sec. For comparison, the actual touchdown velocity experienced by the Apollo 11 Lunar Module was approximately 2 fps. This small impact velocity was due primarily to the crew's electing to delay DPS engine shutoff until footpad contact.

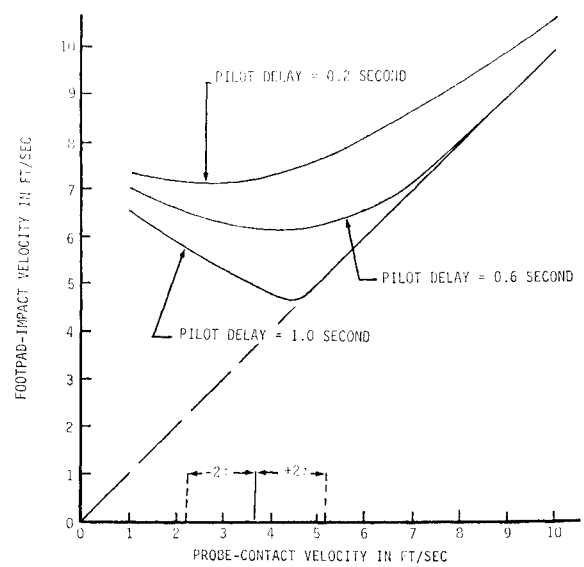

Fig. 5 Relationship between footpad-impact velocity and probe-contact velocity.

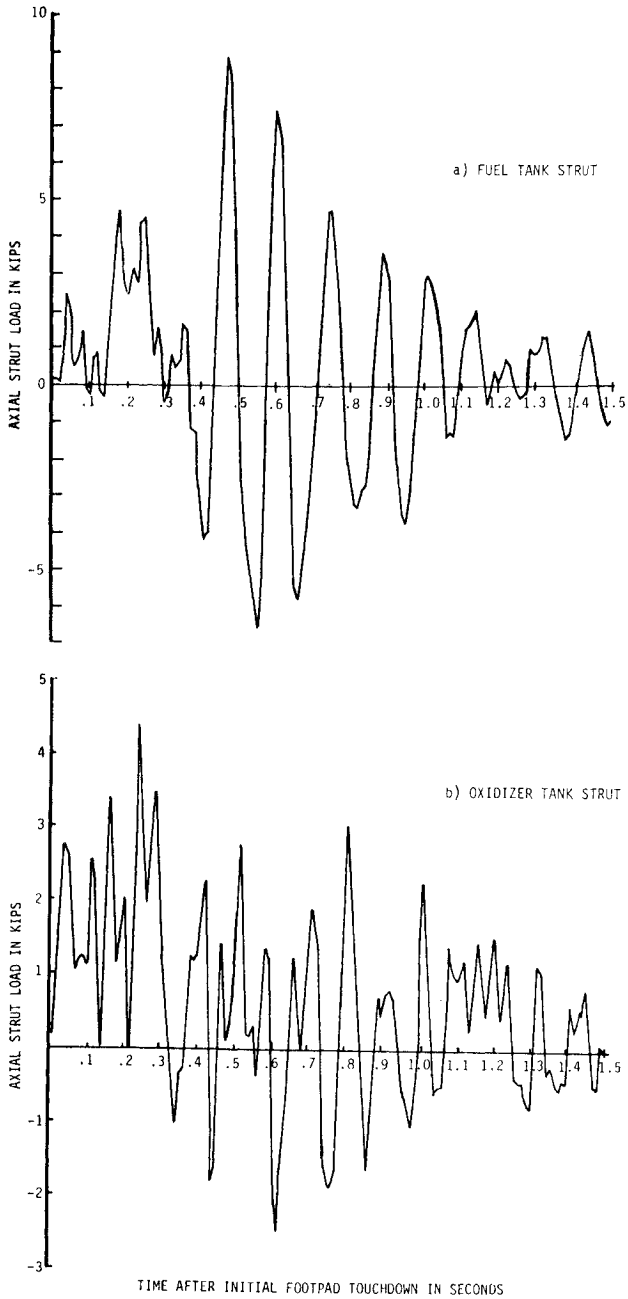

Fig. 6 Load in critical ascent-stage propellant tank support struts.

External dynamic loads for each degree of freedom in the structural model were calculated at intervals of 0.001 sec throughout each landing maneuver. These external load vectors were then used with the stress matrix to compute internal load time histories in 14 critical LM structural elements. Two of the critical structural members were struts supporting the ascent-stage fuel and oxidizer tanks; these two propellant tanks together comprised approximately $\frac{1}{3}$ of the total LM landing weight. The time histories of the axial load in these members are shown in Fig. 6 for the landing case having the maximum tensile load in the fuel tank support strut. Figure 7 shows the corresponding time histories of the longitudinal components of primary landing gear strut forces along with the longitudinal component of LM centroidal acceleration. The maximum internal loads, which are caused primarily by elastic response, are seen for this case to lag the maximum "rigid-body" response. The complicated phasing of the landing-gear strut forces may also be noted in Fig. 7.

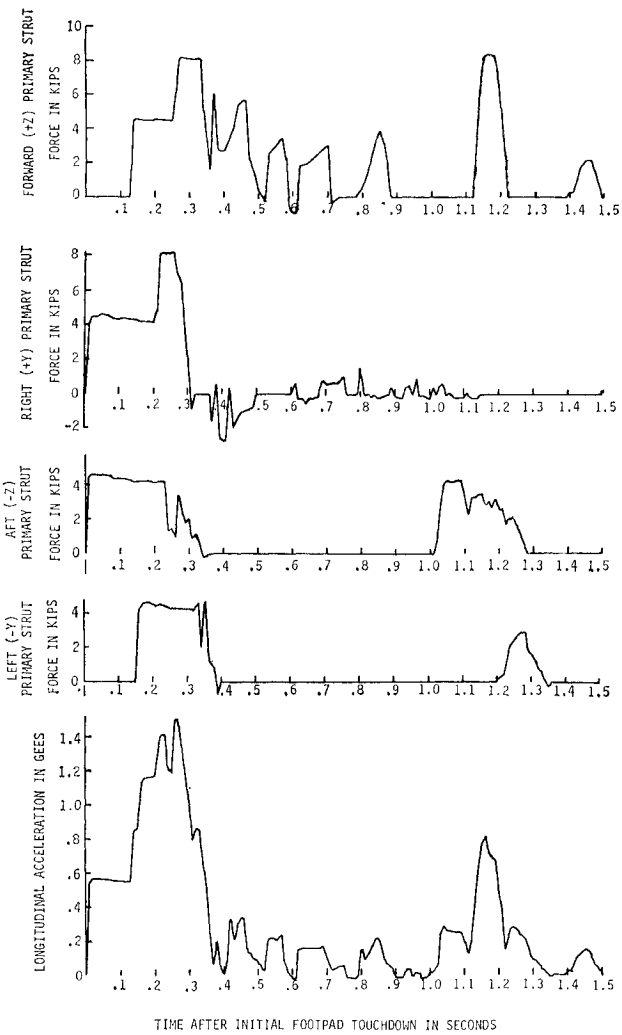

Fig. 7 Longitudinal force in primary struts and LM centroidal acceleration.

An attempt was made to identify a landing case which would cause the worst loads in all the critical structural elements. Because of the complexity of the LM structural model and because of the complicated interaction between the load-causing mechanisms and the LM dynamic response, no such "worst-load" case existed. In fact, for the tensile and compressive loads in the two selected support struts, 14 different landing cases were required to yield the worst five values for each of the four load quantities.

Statistical analyses were performed with the calculated maximum internal load quantities for each landing case. For the nonparametric analysis, the 100 maximum values for each internal load quantity were ordered by magnitude and the corresponding probability levels were calculated by Eq. (5) with confidence level (γ) equal to 95%.

For the parametric analysis, the 100 maximum values for each internal load quantity were analyzed by the chi-square test to justify the assumption of the underlying probability distributions being lognormal. The resulting chi-square exceedance probabilities, which ranged from 0.10 to 0.95, suggested that the assumption of lognormality was acceptable for two reasons. First, the chi-square exceedance probabilities were greater than 10% for all 28 internal load quantities; the chi-square hypothesis is usually accepted for significance levels as low as 1%. Second, if the individual load quantities are statistically independent and if each load quantity is lognormally distributed, then the chi-square probabilities are themselves uniformly distributed over the range (0,1). By the Kolmogorov-Smirnov test, the hy-

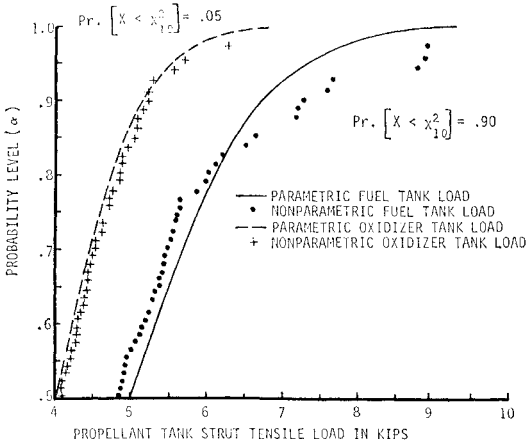

Fig. 8 Comparison of parametric and nonparametric 95% confidence limits.

pothesis of a uniform distribution for the chi-square exceedance probabilities was easily accepted for the 28 samples.

Based on the assumption that the logarithms of the individual load quantities were normally distributed, the parametric confidence limits were calculated by Eq. (12) with 95% confidence. Figure 8 is a plot comparing the parametric and nonparametric confidence limits for the tensile loads in the two ascent-stage propellant tank support struts. The chi-square exceedance probability for the oxidizer tank strut load was 95%; this is reflected by the excellent agreement between the parametric and nonparametric confidence limit curves. The chi-square probability for the fuel tank strut load was a marginal value of 10%. For both load quantities, the largest load in the actual sample corresponds to a nonparametric probability level of 97% with 95% confidence. However, by the extrapolation of the parametric confidence limit, the loads corresponding to higher probability levels may be calculated. In Fig. 8, the loads corresponding to the 99.5% probability level (with 95% confidence) are plotted for both load quantities. The calculated LM internal structural load quantities were all within the structural capability; and the LM design was thereby judged to be adequate for the first lunar landing missions.

Concluding Remarks

Since the Monte Carlo method permits exceedance probabilities to be rationally assigned to the calculated loads, advanced structural criteria involving probability of failure concepts[12] may be utilized. Such criteria may have conceptual advantages over the limit-load/factor-of-safety criteria presently used for structural design.

For this comprehensive lunar landing dynamic loads analysis, the Monte Carlo method was found to be appropriate and very useful. By combining input variables according to their various probability distributions, realistic design verification loads were determined from a relatively small number of simulations. And by means of the parametric confidence limit, loads having low exceedance probabilities were determined efficiently and conservatively from this small sample.

References

[1] Kotanchik, J. N., "NASA-MSC Presentation to LM-5 Critical Design Review," May 1969, Manned Spacecraft Center, Houston, Texas.

[2] Merchant, D. H. and Sawdy, D. T., "LM-5 Lunar Landing Loads Analysis," D2-118255-1, Sept. 1969, The Boeing Co., Houston, Texas.

[3] Hammersley, J. M. and Handscomb, D. C., *Monte Carlo Methods*, Wiley, New York, 1964.

[4] Kahn, H., "Use of Different Monte Carlo Sampling Techniques," *Symposium On Monte Carlo Methods*, Wiley, New York, 1956, pp. 146–190.

[5] Bowker, A. H. and Lieberman, G. J., *Engineering Statistics*, Prentice-Hall, Englewood Cliffs, N.J., 1959.

[6] Bendat, J. and Piersol, A., *Measurement and Analysis of Random Data*, Wiley, New York, 1966.

[7] Lindgren, W. and McElrath, G., *Introduction to Probability and Statistics*, Macmillan, New York, 1959.

[8] Zupp, G. A. and Doiron, H. H., "A Mathematical Procedure for Predicting the Touchdown Dynamics of a Soft-Landing Vehicle," TN D-7045, Sept. 1970, NASA.

[9] Nardone, R. and Wittekind, L., "Results of the LTA-3 Structural Drop Tests," LCQ-560-316A, June 1968, Grumman Aerospace Corp., Bethpage, N.Y.

[10] Pollack, M. and McLaughlin, C., "IIIB LEM Lunar Landing Simulation Studies," LED-470-5, Feb. 1966, Grumman Aerospace Corp., Bethpage, N.Y.

[11] Wiegand, K., "Standard Package for Random Number Generation—SPRANG," AS-2483, Jan. 1967, The Boeing Co., Seattle, Wash.

[12] Ang, A. H.-S. and Amin, M., "Safety Factors and Probability in Structural Design," *Journal of the Structural Division, Transactions of the ASCE*, Vol. 95, No. ST7, July 1969, pp. 1389–1405.